arXiv:astro-ph/0604171v1 7 Apr 2006

ACCEPTED FOR PUBLICATION IN AJ
Preprint typeset using LaTeX style emulateapj v. 6/22/04

DETECTION LIMITS FROM THE MCDONALD OBSERVATORY PLANET SEARCH PROGRAM

ROBERT A. WITTENMYER, MICHAEL ENDL, WILLIAM D. COCHRAN
McDonald Observatory, University of Texas at Austin, Austin, TX 78712

ARTIE P. HATZES
Thüringer Landessternwarte Tautenburg, Sternwarte 5, 07778 Tautenburg, Germany

G. A. H. WALKER, S. L. S. YANG
Physics & Astronomy, University of Victoria, BC V8W 3P6, Canada

DIANE B. PAULSON
NASA/Goddard Space Flight Center, Code 693, Planetary Systems Branch, Greenbelt, MD 20771

Accepted for publication in AJ

ABSTRACT

Based on the long-term radial-velocity surveys carried out with the McDonald Observatory 2.7m Harlan J. Smith Telescope from 1988 to the present, we derive upper limits to long-period giant planet companions for 31 nearby stars. Data from three phases of the McDonald Observatory 2.7m planet-search program have been merged together and for 17 objects, data from the pioneering Canada-France-Hawaii Telescope (CFHT) radial-velocity program have also been included in the companion-limits determination. For those 17 objects, the baseline of observations is in excess of 23 years, enabling the detection or exclusion of giant planets in orbits beyond 8 AU. We also consider the possibility of eccentric orbits in our computations. At an orbital separation of 5.2 AU, we can exclude on average planets of M sin $i \gtrsim 2.0 \pm 1.1$ $\mathrm{M_{Jup}}$ ($e = 0$) and M sin $i \gtrsim 4.0 \pm 2.8$ $\mathrm{M_{Jup}}$ ($e = 0.6$) for 25 of the 31 stars in this survey. However, we are not yet able to rule out "true Jupiters," i.e. planets of M sin $i \sim 1$ $\mathrm{M_{Jup}}$ in 5.2 AU orbits. These limits are of interest for the Space Interferometry Mission (SIM), Terrestrial Planet Finder (TPF), and Darwin missions which will search for terrestrial planets orbiting nearby stars, many of which are included in this work.

Subject headings: stars: planetary systems – extrasolar planets – techniques: radial velocities

1. INTRODUCTION

In the ten years since the discovery of the first extrasolar planet orbiting a main-sequence star (Mayor & Queloz 1995), more than 170 planets have been discovered. The vast majority of these have been detected via high-precision radial-velocity measurements of the planet's gravitational influence on its host star. Current Doppler surveys now routinely achieve precisions of 2-3 m $\mathrm{s^{-1}}$ (e.g. Cochran et al. 2004), facilitating the detection of ever-lower-mass companions, such as the "hot Neptunes" (Bonfils et al. 2005; McArthur et al. 2004; Santos et al. 2004b; Butler et al. 2004) and even "super-Earths" (Rivera et al. 2005).

However, there exists a relatively long record of radial velocity data at somewhat lower precision ($\sim$ 15-20 m $\mathrm{s^{-1}}$) which ought not to be ignored. Such data now cover nearly a quarter-century (Campbell & Walker 1979; Campbell et al. 1988; Walker et al. 1995), and as such are extremely useful in probing nearby stars for long-period giant planets akin to our own Jupiter (orbital period 11.9 years). These data sets are valuable tools in the search for extrasolar analogs to our Solar System. We are now beginning to obtain meaningful answers to some of the following questions: What is the frequency of long-period giant planets in the solar neighborhood? What implications would the lack of such planets have on theories of planet formation? How many planetary systems resemble our own Solar system?

In this work, we merge radial-velocity data from three phases of observations at McDonald Observatory, and we also include data from the CFHT study of Walker et al. (1995). In §2, we describe the data sets, §3 describes the merging procedure and outlines the algorithm used to derive companion limits, and in §4 we present and discuss the constraints these data place on the presence of planets orbiting these stars.

2. OBSERVATIONS

2.1. *A Brief History of Radial Velocity Planet Detection*

Radial-velocity searches for planets around other stars began well before the 1995 discovery of 51 Peg b. Griffin & Griffin (1973) showed that the fundamental limit to the precision of classical radial velocity techniques was not instruments used, but rather was a result of the calibration processes. They pointed out that the optical paths followed by the stellar beam and the separate comparison source illuminated the spectrograph optics differently. Tull (1969) demonstrated how zonal errors in spectrograph optics contribute directly to wavelength (and thus velocity) errors. In addition, thermal and mechanical motion of the spectrograph in the time interval between obtaining the stellar and calibration observations also contributed to the measured velocity er-

Electronic address: robw@astro.as.utexas.edu, mike@astro.as.utexas.edu, wdc@shiraz.as.utexas.edu

rors. Griffin & Griffin (1973) proposed that these sources of errors could be defeated through the calibration of the spectrograph by an absorption line spectrum imposed on the stellar light *before* it entered the spectrograph. They suggested that the use of the very convenient absorptions by the Earth's atmospheric O_2 band at 6300Å would permit stellar radial velocities to be measured to a precision perhaps as good as $0.01\,\mathrm{km\,s^{-1}}$. Campbell & Walker (1979) first used an externally applied absorption spectrum to provide a stable velocity metric for precise radial velocity measurement as applied to planet detection. Instead of the telluric absorption spectrum, they chose to use a stabilized HF gas absorption cell in front of the coudé spectrograph of the Canada France Hawaii Telescope (CFHT). The HF 3-0 R branch lines near 8700Å gave radial velocity precision of $15\,\mathrm{m\,s^{-1}}$ in their twelve-year survey of 21 bright solar-type stars (Campbell et al. 1988; Walker et al. 1995). Although Walker et al. (1995) did not claim any planet detections based on the CFHT data alone, two of their target objects (ϵ Eridani and γ Cephei) were subsequently found to have planetary companions when the CFHT data were combined with McDonald Observatory data (Hatzes et al. 2000, 2003).

The CFHT survey marked the start of a large number of diverse efforts to conduct high-precision radial velocity surveys. At the University of Arizona, McMillan et al. (1985, 1990, 1994) developed a precise radial velocity spectrometer based on the use of a Fabry-Perot etalon in transmission in front of a cross-dispersed echelle spectrograph. This instrument was able to achieve velocity precision of $8\,\mathrm{m\,s^{-1}}$ for bright sources (McMillan et al. 1994), and led to the discovery of the radial velocity variability of K-giants (Smith et al. 1987; Cochran 1988). The idea of using various types of interferometers to obtain precise stellar velocity measurements has been quite popular, with designs proposed by Cochran et al. (1982), Connes (1985), Angel & Woolf (1997), and Ge (2002). Of these designs, only van Eyken et al. (2003) were successful in developing the design into an instrument that actually discovered an extrasolar planet (Ge et al. 2006).

To our knowledge, Beckers (1976) first used the molecular iodine $B^3\Pi^+_{0u}$–$X^1\Sigma^+_g$ band as a velocity reference system, in application to his measurements of the solar rotation. Koch & Woehl (1984) then extended this use of the B-X I_2 band to the measurement of the Doppler shifts of several solar photospheric absorption lines. Libbrecht (1988) then extended the use of I_2 as a velocity metric in searching for p-mode oscillations of α CMi. Marcy & Butler (1992) then implemented the use of the I_2 velocity metric for large-scale precise radial velocity surveys for extrasolar planets. The use of an I_2 cell offers the major advantage that the I_2 lines can be used to measure the spectrometer instrumental profile (Valenti et al. 1995) and thus measure very precise radial velocity variations (Butler et al. 1996). An alternative is to use an optical-fiber fed cross dispersed echelle spectrograph with simultaneous wavelength calibration. This was first done with ELODIE (Baranne et al. 1996) and later with ELODIE (Queloz et al. 2000). To further improve precision with this technique, the HARPS instrument (Rupprecht et al. 2004) is placed in a temperature-stabilized vacuum chamber.

2.2. *The McDonald Observatory Planetary Search Program*

The McDonald Observatory Planetary Search program comprises a large, multifaceted investigation to detect and characterize planetary companions to other stars in our galaxy. It began in 1988 as a high-precision radial velocity survey of bright nearby stars using the McDonald Observatory 2.7m Harlan J. Smith Telescope and coudé spectrograph, but has expanded substantially in size and scope since then. Phase I of the radial velocity planet search program used the telluric O_2 lines near 6300Å as the velocity metric, a technique suggested by Griffin & Griffin (1973). A single order of the McDonald 2.7m telescope coudé echelle spectrograph (cs12) was isolated onto a Texas Instruments 800 × 800 CCD at $R = 210,000$. This system gave about $20\,\mathrm{m\,s^{-1}}$ precision on stars down to $V = 6$, but suffered from systematic velocity errors, possibly due to prevailing atmospheric winds. Diurnal and seasonal variability in the winds introduced spurious periodic signals in the data. We therefore switched to a temperature stabilized I_2 cell as the velocity metric in 1992. This eliminated the systematic errors, and gave a routine radial velocity precision of $\sim 15\,\mathrm{m\,s^{-1}}$. This precision was limited by the 9.6Å bandpass of the single order of the echelle grating, and by the poor charge-transfer and readout properties of the TI 800x800 CCD. To solve these problems, and to achieve substantially improved precision, we began Phase III of the radial velocity program in July 1998, using the same I_2 cell with the newly installed 2dcoudé cross-dispersed echelle spectrograph (Tull et al. 1994) with its 2048x2048 Tektronix CCD. We set up the spectrograph to include echelle orders from 3594Å to 10762Å, which covers the Ca II H and K lines used to measure stellar activity. Wavelength coverage is complete from the blue end to 5691Å, and there are increasingly large inter-order gaps from there to the red end (Tull et al. 1995). Using the full 1200Å bandpass of the I_2 absorption band at the $R = 60,000$ focus of the 2dcoudé allows routine internal precision of 6–$9\,\mathrm{m\,s^{-1}}$ to be achieved. The McDonald program has subsequently been expanded significantly to include a collaboration with Martin Kürster and colleagues on southern hemisphere radial velocity surveys using the facilities of ESO at La Silla and the VLT (Kürster et al. 2000; Endl et al. 2002; Kürster et al. 2003), and a program to use the Keck 1 HIRES spectrograph to search for planetary companions to stars in the Hyades (Cochran et al. 2002; Paulson et al. 2002, 2003, 2004a,b) and in the use of the High Resolution Spectrograph on the Hobby-Eberly Telescope (Cochran et al. 2004). Observations from the McDonald planet search program have been used in the discovery of four planets: 16 Cyg Bb (Cochran et al. 1997), γ Cep Ab (Hatzes et al. 2003), ϵ Eridani b (Hatzes et al. 2000), and HD 13189b (Hatzes et al. 2005). McDonald data were also instrumental in the detection of the brown dwarf HD 137510b (Endl et al. 2004).

2.3. *Observational Data Presented Here*

The majority of the data used in this study were obtained by the McDonald Observatory program Phases I-III using the 2.7m Harlan J. Smith telescope. A list of the target stars is given in Table 1. For 17 of the 31 stars in this study, additional data were available from the CFHT precision radial-velocity work of Walker et al. (1995). Table 2 gives a summary of all four data sets, including the total time span, rms of each data set, and the chromospheric emission ratio log R'_{HK} (Noyes et al. 1984) computed from the McDonald Phase III measurements of the Ca II S-index. The rms values listed in Table 2 include the internal uncertainties of 6–9 $\mathrm{m\,s^{-1}}$ and the velocity jitter inherent to each star.

3. DATA ANALYSIS

3.1. *Merging the Data*

Since each of the four data sets consists of velocities measured relative to an independent and arbitrary zero-point, it was necessary to implement a consistent and robust method of combining them. Before merging, an iterative outlier-rejection routine was applied to each data set separately. Data points which were more than 3.3×RMS from the mean were rejected. This criterion corresponds to a 99.9% confidence level for a Gaussian distribution. The mean and RMS were then recomputed and the outlier rejection was repeated until no more points were rejected. As the targets are well-studied constant-velocity stars, we are confident that we have a well-defined distribution about the mean. For the visual binary 70 Oph A, several velocities were systematically too low due to spectral contamination caused by the chance alignment of both components on the slit, and these points were also removed. The fainter component (Δm = 1.8 mag) adds a Doppler-shifted second spectrum, which distorts the line shapes. Since our velocity computation method assumes a single set of lines, the resultant velocity is skewed by this contamination.

The merging of these data sets was accomplished in the following manner: McDonald Phases II and III are joined with a trial offset, and a least-squares linear fit of a trend of velocity with time is performed on the combination. The offset between the Phase II and III data sets which minimizes the RMS about that linear fit is the one which is applied in order to merge two phases together. This process was then repeated sequentially to join the Phase I and then the CFHT data to the growing data string. The least-squares fitting allows for a linear trend to be present; the merging process was re-done for all non-binaries, this time forcing the slope to be zero (i.e. minimizing the RMS about the mean of the combined data for a grid of trial offsets). The RMS about the mean of data merged in this manner was compared to the RMS about a linear fit to data merged allowing a trend. Since our null hypothesis is that the stars are radial-velocity constants, the method which allowed a slope was only chosen for the 9 stars which showed an improvement in the RMS of the merged data set when a slope was allowed. Those stars were: η Cep, η Cas, α For, θ UMa, ξ Boo A, μ Her, 70 Oph A, and 61 Cyg A & B. All of these stars are well-known long-period binaries, so the use of a slope was justified.

The orbital periods of these 9 known binaries were sufficiently long that a simple linear approximation was sufficient, except for μ Her, ξ Boo A (quadratic trend) and 70 Oph A (Keplerian solution). Fits to these trends were subtracted from the data sets and the residuals were used as input for the detection-limit algorithm. The three data sets on the visual binary μ Her were merged in a similar manner. The binary period (43.2 years; Worley & Heintz 1995) is such that a linear trend is a suboptimal approximation for the purposes of merging the 16.9 years of data, and a quadratic fit was used to approximate the shape of the orbit. This procedure was also used for ξ Boo A; the data and fits are shown in Figure 1. For 70 Oph A, the quadratic approximation was still insufficient, as the 16.1 years of available data represents a significant portion of the 91.44 year published orbital period (Batten et al. 1984), and an orbital solution for the binary system had to be obtained using GaussFit (Jefferys et al. 1987). The solution to the combined data set (McDonald Phases I-III plus much lower-precision data from Batten et al. 1984) is given in Table 3, and plotted in Figure 2. The large uncertainties in the fitted parameters are due to the fact that the available data do not encompass a complete orbit, and hence the model is poorly constrained. The fitted value of ω was derived by a rudimentary grid search around the published value, as GaussFit would not converge with ω as a free parameter. The orbital parameters of the binary system are substantially different than those reported in Batten et al. (1984), likely owing to the fact that the McDonald velocities, which are an order of magnitude more precise, drive the fit. Only the McDonald data were used in the computation of companion limits for 70 Oph A.

3.2. *Periodogram Analysis*

After the data sets were merged together, and trends due to binary orbits were subtracted, we searched for periodicities using a Lomb-Scargle periodogram (Lomb 1976; Scargle 1982). False alarm probabilities (FAP) were established using a bootstrap randomization method as described in Kürster et al. (1997) and Endl et al. (2002). This bootstrap method, unlike the nominal analytic FAP formula of Scargle (1982), makes no assumptions about the distribution of the data; rather, the error distribution of the actual data themselves is used. The periodogram search interval was from 2 days up to the full extent of observations for each object. We used 10,000 bootstrap randomizations to determine the FAP of the highest peak in the periodogram for each star; the results are given in Table 4. Only one star had a periodicity with a significance greater than 99%: π^3 Ori, with a peak at 73.26 days and a bootstrap FAP of 0.8%. As this is an active early-type (F6V) star, we are confident that this is due to a combination of stellar activity and reduced velocity precision (from the paucity of lines) rather than the presence of a companion. Additionally, no peak was evident in a periodogram on the more precise McDonald Phase III data alone, supporting our conclusion that it is a spurious noise spike.

3.3. *Determination of Companion Limits*

Companion limits were determined via an algorithm which injected test signals into the data, and then attempted to recover that signal using a periodogram search. Test signals were generated using the method of Lehmann-Filhés (Lehmann-Filhés 1894) as described in Binnendijk (1960):

$$V_r = \gamma + K[e\ cos\ \omega + cos(\nu + \omega)], \qquad (1)$$

where V_r is the radial velocity, γ is the systemic velocity, K is the velocity semiamplitude, e the orbital eccentricity, ω the argument of periastron, and ν the true anomaly. In the above equation, ν can be expressed in terms of observables via the following relations:

$$tan\ \frac{\nu}{2} = \left[\frac{(1+e)}{(1-e)}\right]^{1/2} tan\ \frac{E}{2} \qquad (2)$$

and

$$M = \frac{2\pi}{P}(t - T_0) = E - e\ sin\ E, \qquad (3)$$

for a signal with period P, periastron passage time T_0, observation time t, mean anomaly M, and eccentric anomaly E. For each data set, the algorithm stepped through 300 trial periods at even steps in the logarithm between 2 days and the total duration of observations. At each trial period, the program sampled 30 phase steps of the periastron time T_0, and for nonzero eccentricities, sampled 36 values of the argument of periastron ω at intervals of 10 degrees. The velocity semi-amplitude K of the test signal was allowed to vary from 10 to 1000 m s^{-1}. The systemic velocity γ of each combined data set was forced to be equal to zero. For each set of Keplerian orbital parameters, synthetic radial velocities were generated using the observation times from the input data. This simulated signal was then added to the data, and a Lomb-Scargle periodogram was used to attempt to recover that signal. For a signal to count as having been recovered, the periodogram's highest peak had to occur at the correct period with a FAP of less than 0.1%. The FAP was estimated using the formula from Horne & Baliunas (1986). For each K velocity, 99% of the 1080 test signals[1] had to be recovered in this manner in order for that velocity semiamplitude (corresponding to a planet of a given mass at a given semimajor axis) to be considered "ruled out" by the data. If more than 1% of the orbital configurations tested at a given K value were *not* ruled out in this manner, the algorithm increased K by 1 m s^{-1} and repeated the process until it was able to recover 99% of the parameter configurations (e, ω, T_0) that were tested. Once this occurred, the planetary mass ruled out was computed by the following:

$$M_2\ sin\ i = (1-e^2)^{1/2}\left[(1.036\times10^{-7})M_1^2 P K^3\right]^{1/3}, \quad (4)$$

where M_1 is the stellar mass in solar masses, P is the orbital period in days, K is the radial-velocity semiamplitude in km s^{-1}, and M_2 sin i is the projected planetary mass in solar masses. The algorithm then moved to the next trial period and repeated the entire process.

Unlike most previous companion limit determinations (Murdoch et al. 1993; Walker et al. 1995; Nelson & Angel 1998; Cumming et al. 1999; Endl et al. 2002), this procedure allows for nonzero eccentricities in the trial orbits (but see Desidera et al. 2003). For the eccentric case, a value of $e = 0.6$ was chosen; of the known extrasolar planets, 90% have $e < 0.6$ Marcy et al. (2005). Allowing higher eccentricities substantially reduced the ability to rule out the test signals, as the sporadic sampling of the data would likely miss the relatively high-velocity points near periastron. Figure 3 shows the effect of allowing various ranges of eccentricity. Note that although the limits derived by this study are rendered somewhat less stringent by the inclusion of nonzero eccentricities, the effect is relatively minor for our adopted value of $e = 0.6$. Allowing a larger range of eccentricities (up to $e = 0.9$), however, substantially reduces the sensitivity of the companion-limit determination, as demonstrated in Figure 3. We emphasize that the upper limits derived by the method described above are much more stringent, and hence will result in higher companion-mass limits than those reported by previous studies.

4. RESULTS AND DISCUSSION

Limits to planetary companions derived using these data are shown in Figures 4-11. In each panel, the lower set of points (solid line) represents the companion limits for the zero-eccentricity case, and the dotted line is for the case of $e = 0.6$. Notably, despite the abundance and quality of data available in this study, we are as yet unable to rule out *any* planets with M sin $i \lesssim 1$ $M_{\rm Jup}$ in 5.2 AU orbits with eccentricities as large as $e = 0.6$. When only circular orbits are considered, such objects can be ruled out for τ Ceti, σ Dra, 61 Cyg A, and 61 Cyg B. Table 5 lists the minimum planet masses that can be excluded by these data at selected semimajor axes, for the $e = 0$ and $e = 0.6$ cases. The results given in Table 5 are shown in histogram format in Figure 12, which indicates that for most stars in this survey, Saturn-mass planets in close orbits ($a \sim 0.1$ AU) can be ruled out.

It is also useful to consider the effect of giant planets in intermediate orbits ($a \sim 2-3$ AU) which may perturb lower-mass planets within the habitable zone of the star. If such objects can be excluded with confidence, their host stars become attractive candidates for the *Terrestrial Planet Finder* (TPF) and Darwin missions, which aim to detect Earth-like planets in the habitable zone. Menou & Tabachnik (2003) defined a planet's zone of influence to extend from $R_{in} = (1-e)a - 3R_{Hill}$ to $R_{out} = (1+e)a + 3R_{Hill}$, where the Hill radius is

$$R_{Hill} = a\left(\frac{M_p}{3M_*}\right)^{1/3}, \qquad (5)$$

and e is the planet's eccentricity, a is its semimajor axis, M_p is its mass, and M_* is the mass of the star. Simulations by Menou & Tabachnik (2003) demonstrated that terrestrial planets were nearly always ejected or consumed in systems where an eccentric giant planet's zone of influence overlapped the habitable zone. We can then ask whether the companion limits derived in this work can be used to exclude such perturbing bodies. Such a pursuit is limited by the fact that even distant giant planets can disrupt the habitable zone if their orbits are sufficiently eccentric, and as shown in Figure 1, the nature of the radial-velocity data is such that we are least sensitive to the most eccentric planets. Nevertheless, for small eccentricities ($e \lesssim 0.2$), it is possible to combine these dynamical calculations with our companion-limit determinations to define a "safe zone": a region of parameter space in which we can exclude perturbing giant planets exterior to the habitable zone. For such regions, the possibility of terrestrial planets in the habitable zone remains open for programs such as TPF and Darwin. In Figures 4-11, the region to the left of the dot-dashed line and above the dotted line defines the "safe zone" for perturbing outer giant planets with $e < 0.2$. These were only plotted for main-sequence stars, using the definition of the "continuously habitable zone" given in Kasting et al. (1993). The region left of the dot-dashed line and *below* our limits represents a set of potentially dangerous objects which would disrupt the habitable zone, yet be undetectable with the current data. Higher eccentricities would push the dot-dashed line to the right and reduce its slope, such that for perturbers with $e \gtrsim 0.5$, our limits computations can say nothing about such objects (i.e. the curves would not intersect). The companion limits we have derived thus place some constraints on potentially disruptive objects in these systems, which will assist in target selection for the TPF and Darwin missions.

---

[1] For signals with $e = 0$, *all* 30 variations in T_0 had to be recovered, as ω had no meaning.

Noting that the Phase III data are of substantially higher quality than the previous data sets, we asked what velocity rms would be required to rule out a Jupiter analog orbiting a solar-type star. We generated simulated observations consisting of Gaussian noise at the actual observation times (spanning 16 years) for 16 Cyg A, the star in this study which is closest in spectral type (G1.5 V) to our Sun. Figure 13 shows the results of the companion-limit algorithm on four of these simulated data sets with four levels of rms scatter. In order to rule out a planet with M sin i of 1 $M_{\rm Jup}$ in a 5.2 AU orbit ($e = 0.1$), the data need to have an rms less than about 10 m s^{-1}. The rms of Phase III observations of 16 Cyg A is 6.9 m s^{-1} over a period of 6.3 years, whereas the complete 16 years has an overall rms of 26.8 m s^{-1}. Hence, a Jupiter analog could be ruled out for 16 Cyg A with about 10 more years of data of the same quality as McDonald Phase III. The weighted mean rms of all McDonald Phase III observations in this survey is 12.6 m s^{-1}. Eleven stars (see Table 2) currently achieve a Phase III rms better than 8 m s^{-1}; this represents one-third of the stars discussed in this work. These simulations show that the average precision of Phase III needs to be improved by about 2-3 m s^{-1} in order to achieve the sensitivity required to detect or exclude Jupiter analogs for all of these stars.

5. SUMMARY

We have amassed a substantial quantity of radial-velocity data on 31 nearby stars, spanning up to 23 years of observations. We have applied a robust method to place conservative limits on planetary companions orbiting these stars. We have considered the effect of eccentric orbits in our computations, which better reflects the diversity of known extrasolar planetary systems. Saturn-mass planets within 0.1 AU can be ruled out for nearly all of these stars. At 5.2 AU, we can exclude on average planets with M sin $i \gtrsim 2.0 \pm 1.1$ $M_{\rm Jup}$ ($e = 0$)and M sin $i \gtrsim 4.0 \pm 2.8$ $M_{\rm Jup}$ ($e = 0.6$) for 25 of the 31 stars. Although we now have a quite sufficient time baseline for the detection of Jupiter analogs in ~12 year orbits, we find that the overall velocity precision is not yet sufficient to exclude Jupiter-mass planets at 5.2 AU. However, improvements in the current McDonald Observatory 2.7m telescope planet search program put the desired level of precision within reach for inactive stars.

This research was supported by NASA grants NNG04G141G and NNG05G107G. R.W. acknowledges support from the Sigma Xi Grant-in-Aid of Research and the Texas Space Grant Consortium. D.B.P. is currently a National Research Council fellow working at NASA's Goddard Space Flight Center. We are grateful to Barbara McArthur for her assistance with GaussFit software, and to E.L. Robinson for insightful comments which improved this manuscript. This research has made use of NASA's Astrophysics Data System (ADS), and the SIMBAD database, operated at CDS, Strasbourg, France, as well as computing facilities at San Diego State University.

REFERENCES

Allende Prieto, C., & Lambert, D. L. 1999, A&A, 352, 555
Angel, J. R. P., & Woolf, N. J. 1997, ApJ, 475, 373
Batten, A. H., Fletcher, J. M., & Campbell, B. 1984, PASP, 96, 903
Baranne, A., et al. 1996, A&AS, 119, 373
Beckers, J. M. 1976, Nature, 260, 227
Binnendijk, L. 1960, Philadelphia, University of Pennsylvania Press [1960]
Bonfils, X., et al. 2005, A&A, 443, L15
Butler, R. P., Vogt, S. S., Marcy, G. W., Fischer, D. A., Wright, J. T., Henry, G. W., Laughlin, G., & Lissauer, J. J. 2004, ApJ, 617, 580
Butler, R. P., Marcy, G. W., Williams, E., McCarthy, C., Dosanjh, P., & Vogt, S. S. 1996, PASP, 108, 500
Campbell, B., Walker, G. A. H., & Yang, S. 1988, ApJ, 331, 902
Campbell, B., & Walker, G. A. H. 1979, PASP, 91, 540
Cochran, W. D. 1988, ApJ, 334, 349
Cochran, W. D., Hatzes, A. P., Butler, R. P., & Marcy, G. W. 1997, ApJ, 483, 457
Cochran, W. D., Hatzes, A. P., & Paulson, D. B. 2002, AJ, 124, 565
Cochran, W. D., Smith, H. J., & Smith, W. H. 1982, Proc. SPIE, 331, 315
Cochran, W. D., et al. 2004, ApJ, 611, L133
Connes, P. 1985, Ap&SS, 110, 211
Cumming, A., Marcy, G. W., & Butler, R. P. 1999, ApJ, 526, 890
Desidera, S., et al. 2003, A&A, 405, 207
do Nascimento, J. D., Canto Martins, B. L., Melo, C. H. F., Porto de Mello, G., & De Medeiros, J. R. 2003, A&A, 405, 723
Endl, M., Hatzes, A. P., Cochran, W. D., McArthur, B., Allende Prieto, C., Paulson, D. B., Guenther, E., & Bedalov, A. 2004, ApJ, 611, 1121
Endl, M., Kürster, M., Els, S. H. A. P., Cochran, W. D., Dennerl, K., Döbereiner, S. 2002, A&A, 392, 671
Endl, M., Kürster, M., & Els, S. 2000, A&A, 362, 585
Fernandes, J., Lebreton, Y., Baglin, A., & Morel, P. 1998, A&A, 338, 455
Ge, J., et al. 2006, ApJ, submitted
Ge, J. 2002, ApJ, 571, L165
Griffin, R., & Griffin, R. 1973, MNRAS, 162, 255
Hatzes, A. P., Guenther, E. W., Endl, M., Cochran, W. D., Döllinger, M. P., & Bedalov, A. 2005, A&A, 437, 743
Hatzes, A. P., et al. 2000, ApJ, 544, L145
Hatzes, A. P., Cochran, W. D., Endl, M., McArthur, B., Paulson, D. B., Walker, G. A. H., Campbell, B., & Yang, S. 2003, ApJ, 599, 1383
Horne, J. H., & Baliunas, S. L. 1986, ApJ, 302, 757
Jefferys, W. H., Fitzpatrick, M. J., & McArthur, B. E. 1987, Celestial Mechanics, 41, 39
Kasting, J. F., Whitmire, D. P., & Reynolds, R. T. 1993, Icarus, 101, 108
Koch, A., & Woehl, H. 1984, A&A, 134, 134
Kürster, M., et al. 2003, A&A, 403, 1077

TABLE 1
TARGET LIST AND STELLAR PARAMETERS

Star	HR	Spec. Type	V magnitude	Mass ($M_\odot$)	Reference for Mass Estimate
η Cas	219	G0V	3.44	0.90	Allende Prieto & Lambert (1999)
τ Cet	509	G8V	3.50	0.65	Santos et al. (2004a)
θ Per	799	F8V	4.12	1.15	Allende Prieto & Lambert (1999)
ι Per	937	G0V	4.04	1.23	Allende Prieto & Lambert (1999)
α For	963	F8V	3.87	1.30	Allende Prieto & Lambert (1999)
κ^1 Cet	996	G5V	4.82	1.05	Allende Prieto & Lambert (1999)
δ Eri	1136	K0IV	3.54	0.96	Allende Prieto & Lambert (1999)
o^2 Eri	1325	K1V	4.43	0.65	Santos et al. (2004a)
π^3 Ori	1543	F6V	3.19	1.24	Allende Prieto & Lambert (1999)
λ Aur	1729	G1.5IV-V	4.71	1.15	Allende Prieto & Lambert (1999)
θ UMa	3775	F6IV	3.17	1.53	Allende Prieto & Lambert (1999)
36 UMa	4112	F8V	4.82	1.14	Allende Prieto & Lambert (1999)
β Vir	4540	F8V	3.61	1.36	Allende Prieto & Lambert (1999)
β Com	4983	G0V	4.28	1.05	Allende Prieto & Lambert (1999)
61 Vir	5019	G6V	4.75	1.01	Allende Prieto & Lambert (1999)
ξ Boo A	5544	G8V	4.55	0.86	Fernandes et al. (1998)
λ Ser	5868	G0V	4.43	0.97	Allende Prieto & Lambert (1999)
γ Ser	5933	F6V	3.85	1.28	Allende Prieto & Lambert (1999)
36 Oph A	6402	K1V	5.29	0.78	Walker et al. (1995)
μ Her	6623	G5IV	3.42	1.10	do Nascimento et al. (2003)
70 Oph A	6752	K0V	4.03	0.97	Allende Prieto & Lambert (1999)
σ Dra	7462	K0V	4.68	0.85	Nelson & Angel (1998)
16 Cyg A	7503	G1.5V	5.96	0.98	Allende Prieto & Lambert (1999)
31 Aql	7373	G8IV	5.16	0.95	do Nascimento et al. (2003)
β Aql	7602	G8IV	3.71	1.50	do Nascimento et al. (2003)
γ^2 Del	7948	K1IV	4.27	1.90	do Nascimento et al. (2003)
η Cep	7957	K0IV	3.43	1.39	Allende Prieto & Lambert (1999)
61 Cyg A	8085	K5V	5.21	0.67	Walker et al. (1995)
61 Cyg B	8086	K7V	6.03	0.59	Walker et al. (1995)
HR 8832	8832	K3V	5.56	0.79	Nelson & Angel (1998)
ι Psc	8969	F7V	4.13	1.38	Allende Prieto & Lambert (1999)

Kürster, M., Endl, M., Els, S., Hatzes, A. P., Cochran, W. D., Döbereiner, S., & Dennerl, K. 2000, A&A, 353, L33

Kürster, M., Schmitt, J. H. M. M., Cutispoto, G., & Dennerl, K. 1997, A&A, 320, 831

Lehmann-Filhés, R. 1894, *Astronomische Nachrichten*, 136, 17

Libbrecht, K. G. 1988, IAU Symp. 132: The Impact of Very High S/N Spectroscopy on Stellar Physics, 132, 83

Lomb, N. R. 1976, Ap&SS, 39, 447

Marcy, G., Butler, R. P., Fischer, D., Vogt, S., Wright, J. T., Tinney, C. G., & Jones, H. R. A. 2005, Progress of Theoretical Physics Supplement, 158, 24

Marcy, G. W., & Butler, R. P. 1992, PASP, 104, 270

Mayor, M., & Queloz, D. 1995, Nature, 378, 355

McArthur, B. E., et al. 2004, ApJ, 614, L81

McMillan, R. S., Smith, P. H., Frecker, J. E., Merline, W. J., & Perry, M. L. 1985, IAU Colloq. 88: Stellar Radial Velocities, 63

McMillan, R. S., Smith, P. H., Perry, M. L., Moore, T. L., & Merline, W. J. 1990, Proc. SPIE, 1235, 601

McMillan, R. S., Moore, T. L., Perry, M. L., & Smith, P. H. 1994, Ap&SS, 212, 271

Menou, K., & Tabachnik, S. 2003, ApJ, 583, 473

Murdoch, K. A., Hearnshaw, J. B., & Clark, M. 1993, ApJ, 413, 349

Nelson, A. F., & Angel, J. R. P. 1998, ApJ, 500, 940

Noyes, R. W., Hartmann, L. W., Baliunas, S. L., Duncan, D. K., & Vaughan, A. H. 1984, ApJ, 279, 763

Paulson, D. B., Cochran, W. D., & Hatzes, A. P. 2004, AJ, 127, 3579

Paulson, D. B., Saar, S. H., Cochran, W. D., & Henry, G. W. 2004, AJ, 127, 1644

Paulson, D. B., Sneden, C., & Cochran, W. D. 2003, AJ, 125, 3185

Paulson, D. B., Saar, S. H., Cochran, W. D., & Hatzes, A. P. 2002, AJ, 124, 572

Queloz, D., et al. 2000, A&A, 354, 99

Rivera, E. J., et al. 2005, ApJ, 634, 625

Rupprecht, G., et al. 2004, Proc. SPIE, 5492, 148

Santos, N. C., Israelian, G., & Mayor, M. 2004, A&A, 415, 1153

Santos, N. C., et al. 2004, A&A, 426, L19

Scargle, J. D. 1982, ApJ, 263, 835

Smith, P. H., McMillan, R. S., & Merline, W. J. 1987, ApJ, 317, L79

Tull, R. G. 1969, Appl. Opt., 8, 1635

Tull, R. G., MacQueen, P., Sneden, C., & Lambert, D. L. 1994, ASP Conf. Ser. 55: Optical Astronomy from the Earth and Moon, 55, 148

Tull, R. G., MacQueen, P. J., Sneden, C., & Lambert, D. L. 1995, PASP, 107, 251

Valenti, J. A., Butler, R. P., & Marcy, G. W. 1995, PASP, 107, 966

van Eyken, J. C., Ge, J. C., Mahadevan, S., DeWitt, C., & Ren, D. 2003, Proc. SPIE, 5170, 250

Walker, G. A. H., Walker, A. R., Irwin, A. W., Larson, A. M., Yang, S. L. S., & Richardson, D. C. 1995, Icarus, 116, 359

Worley, C. E., & Heintz, W. D. 1995, VizieR Online Data Catalog, 5039, 0

TABLE 2
Summary of Observations

Star	N	T (years)	CFHT rms (m s^{-1})	Phase I rms (m s^{-1})	Phase II rms (m s^{-1})	Phase III rms (m s^{-1})	log R'_{HK}
η Cas	131	16.3	···	28.1	28.9	7.3	-4.926
τ Cet	183	23.3	14.2	22.3	28.7	10.4	-4.979
θ Per	65	9.5	···	···	59.6	17.9	-4.919
ι Per	165	23.9	18.2	30.0	18.6	10.2	-5.041
α For	66	15.3	···	28.9	41.3	15.8	-5.023
κ^1 Cet	134	23.0	23.7	34.4	29.7	20.1	-4.441
δ Eri	109	16.1	···	17.8	22.5	9.4	-5.228
o^2 Eri	138	22.1	18.6	30.4	18.0	14.6	-4.951
π^3 Ori	160	15.9	···	169.9	113.3	26.4	-4.716
λ Aur	63	10.4	···	···	20.6	10.1	-5.051
θ UMa	268	18.3	18.8	43.1	43.7	14.8	-5.608
36 UMa	194	23.0	21.0	19.4	22.4	8.2	-4.811
β Vir	205	23.3	28.4	30.5	32.6	7.6	-4.942
β Com	191	22.4	18.4	31.7	42.0	11.1	-4.749
61 Vir	149	23.0	18.4	25.8	31.0	7.8	-5.030
ξ Boo A	186	23.3	23.6	34.5	31.9	23.3	-4.420
λ Ser	63	11.5	···	···	7.9	19.4	-4.936
γ Ser	149	15.1	···	84.7	41.6	25.6	-4.934
36 Oph A	91	21.9	20.1	21.5	33.1	16.3	-4.614
μ Her	173	16.9	···	28.4	24.4	9.2	-5.092
70 Oph A	98	16.2	···	111.4	43.3	17.4	-4.736
σ Dra	178	23.6	14.5	21.5	23.1	9.9	-4.865
16 Cyg A	102	16.0	···	34.4	29.0	6.9	-5.018
31 Aql	38	7.9	···	···	22.5	11.9	-5.123
β Aql	183	22.1	14.6	28.0	20.1	16.4	-5.171
γ^2 Del	103	15.0	···	23.7	21.7	16.8	-5.354
η Cep	187	23.5	19.2	29.5	16.4	9.6	-5.223
61 Cyg A	143	23.4	20.7	22.3	13.5	7.2	-4.862
61 Cyg B	121	22.4	16.9	23.5	16.2	3.9	-4.962
HR 8832	119	22.9	14.9	22.8	13.8	12.9	-5.013
ι Psc	54	11.2	···	···	26.4	10.3	-4.915

TABLE 3
Orbital Solution for 70 Oph A

Parameter	Estimate	Uncertainty
Period (years)	179.1	99.5
T_0 (HJD)	2445610.22	91.74
e	0.69	0.11
ω (degrees)	193.6	···
K_A (m s^{-1})	4163	257

TABLE 4
Results of Periodogram Analysis

Star	Period (days)	FAP
η Cas	2.964	0.296
τ Cet	8.389	0.034
θ Per	348.432	0.443
ι Per	91.996	0.027
α For	8.262	0.395
κ^1 Cet	33.069	0.034
δ Eri	22.051	0.788
o^2 Eri	7.463	0.900
π^3 Ori	73.260	0.008
λ Aur	2.549	0.188
θ UMa	2.587	0.178
36 UMa	3703.704	0.694
β Vir	3.307	0.262
β Com	9.946	0.315
61 Vir	9.777	0.072
ξ Boo A	6.298	0.202
λ Ser	4.929	0.773
γ Ser	8.961	0.137
36 Oph A	2.641	0.565
μ Her	7.623	0.039
70 Oph A	6.138	0.989
σ Dra	30.553	0.109
16 Cyg A	2.873	0.038
31 Aql	8.374	0.536
β Aql	2.800	0.019
γ^2 Del	3.837	0.099
η Cep	5.940	0.030
61 Cyg A	6.570	0.159
61 Cyg B	6.872	0.846
HR 8832	25.227	0.144
ι Psc	2.499	0.144

TABLE 5
Minimum-Mass Companion Limits

Star	M sin i ($M_{\rm Jup}$) 0.05 AU $e = 0.0$	M sin i ($M_{\rm Jup}$) 0.1 AU $e = 0.0$	M sin i ($M_{\rm Jup}$) 3 AU $e = 0.6$	M sin i ($M_{\rm Jup}$) 3 AU $e = 0.0$	M sin i ($M_{\rm Jup}$) 5.2 AU $e = 0.6$	M sin i ($M_{\rm Jup}$) 5.2 AU $e = 0.0$
η Cas	0.13	0.17	1.30	0.87	2.31	1.37
τ Cet	0.09	0.16	1.14	0.67	1.34	0.90
θ Per	0.48	0.62	5.71	3.46	···	···
ι Per	0.12	0.16	1.46	0.95	2.70	1.69
α For	0.32	0.57	6.12	3.05	8.46	4.37
κ^1 Cet	0.18	0.27	2.34	1.44	3.81	2.05
δ Eri	0.13	0.19	2.10	1.07	12.74	1.88
o^2 Eri	0.12	0.16	1.33	0.88	1.66	1.16
π^3 Ori	0.84	1.51	9.79	6.01	46.70	8.54
λ Aur	0.18	0.24	2.19	1.25	···	···
θ UMa	0.24	0.36	3.09	1.96	4.60	2.57
36 UMa	0.13	0.17	1.46	0.91	2.54	1.71
β Vir	0.16	0.23	2.49	1.57	4.19	2.61
β Com	0.16	0.26	1.95	1.24	3.29	2.22
61 Vir	0.14	0.20	1.62	1.16	2.58	1.69
ξ Boo A	0.16	0.19	2.00	1.24	2.61	1.78
λ Ser	0.16	0.21	2.01	1.14	···	···
γ Ser	0.44	0.49	4.15	2.97	10.89	5.80
36 Oph A	0.19	0.23	2.24	1.39	5.83	2.33
μ Her	0.14	0.21	1.53	0.96	2.55	1.52
70 Oph A	0.46	0.84	8.71	5.04	12.78	7.19
σ Dra	0.11	0.12	1.12	0.79	1.60	1.03
16 Cyg A	0.18	0.32	2.21	1.38	5.44	2.45
31 Aql	0.22	0.38	··· [a]	1.90	···	···
β Aql	0.12	0.18	1.61	1.04	2.67	1.77
γ^2 Del	0.22	0.32	2.55	1.60	4.70	2.32
η Cep	0.13	0.17	2.02	0.86	2.41	1.52
61 Cyg A	0.09	0.14	1.60	0.85	2.10	0.98
61 Cyg B	0.07	0.10	1.12	0.66	1.48	0.80
HR 8832	0.11	0.14	1.65	0.81	2.56	1.14
ι Psc	0.26	0.38	4.35	1.85	4.91	2.64

[a] Too few data points for a reliable periodogram search, due to undersampling of eccentric test signals.

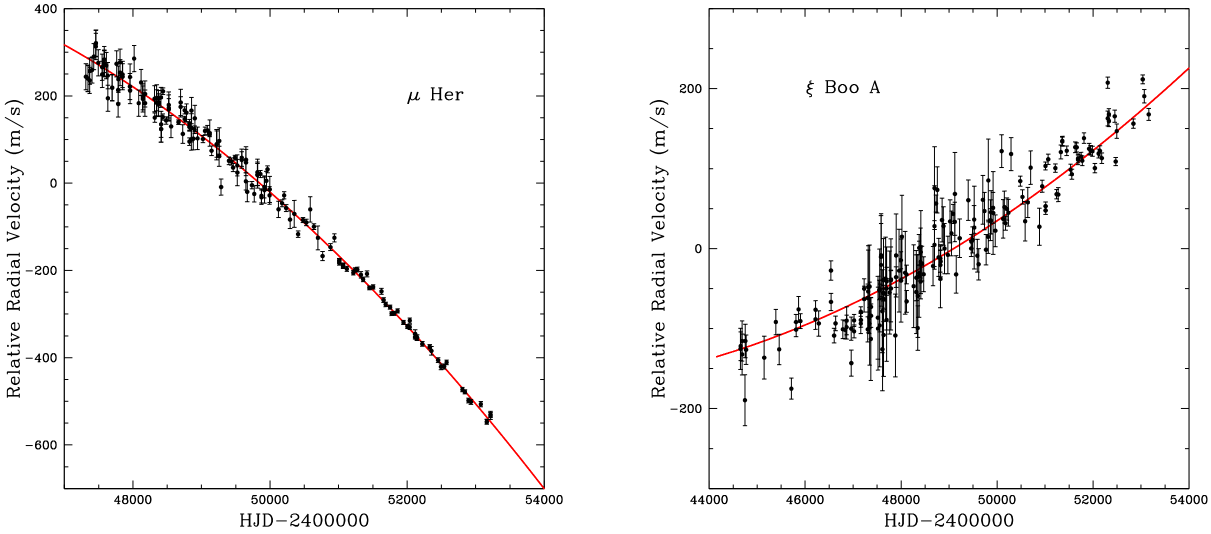

FIG. 1.— Quadratic fits to μ Her data (left panel) and ξ Boo A (right panel).

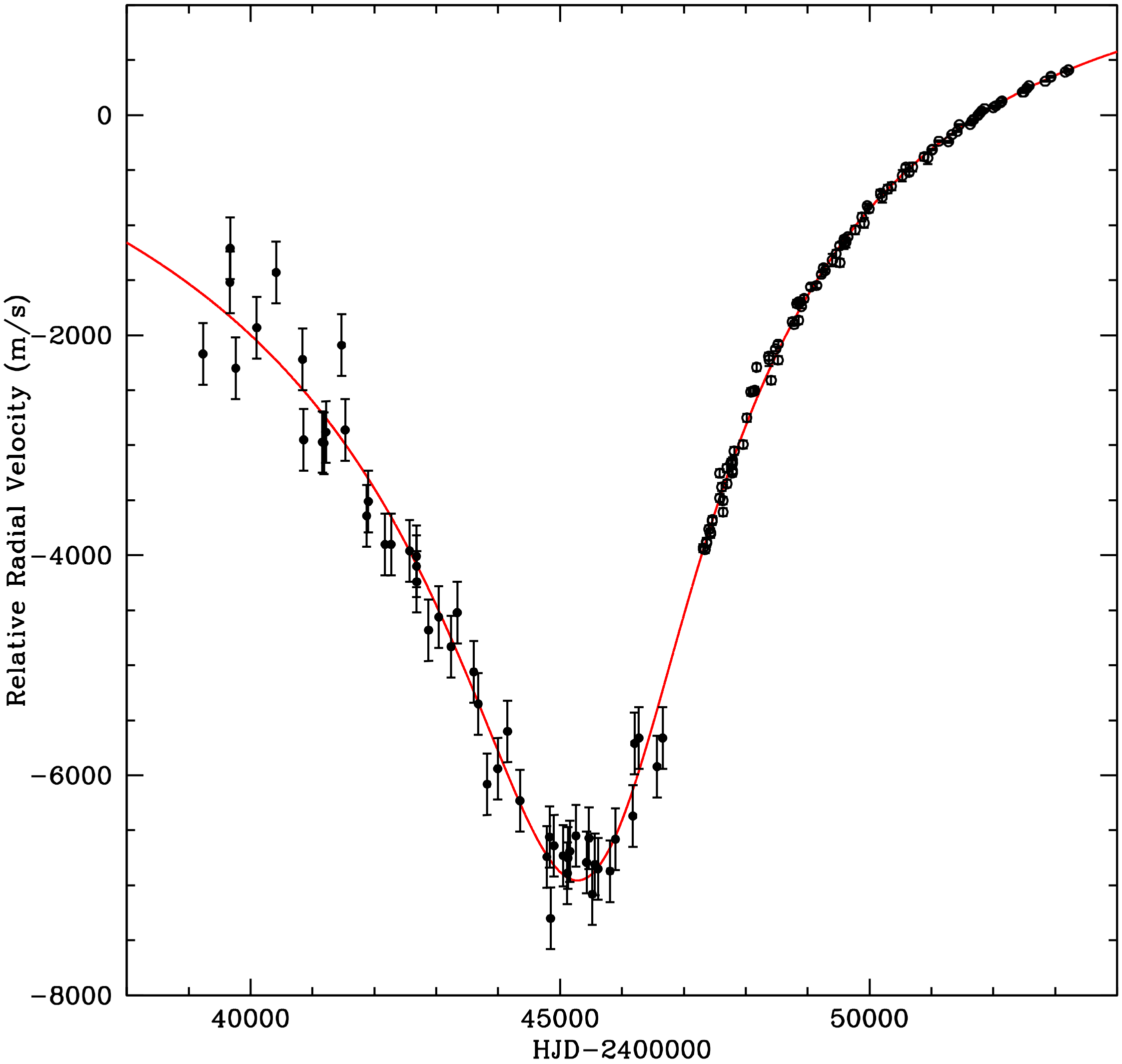

Fig. 2.— Orbital solution for the visual binary 70 Oph A using data from Batten et al. (1984) (filled circles) and McDonald Observatory phase I-III (open circles).

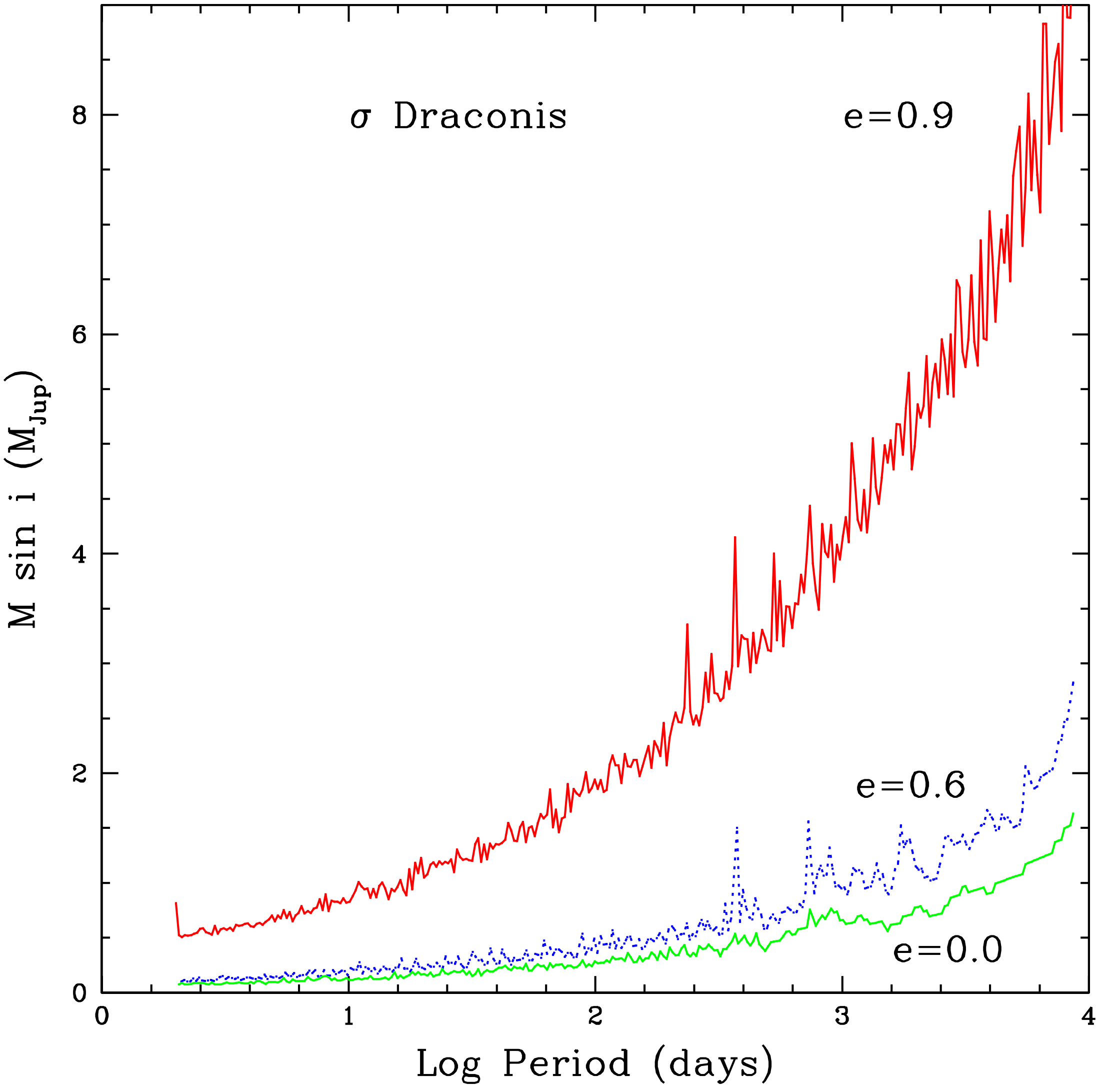

FIG. 3.— The effect of eccentricity on limit determinations. Allowing higher eccentricities reduces the sensitivity somewhat, due to the increased probability of unfortunately-phased observations.

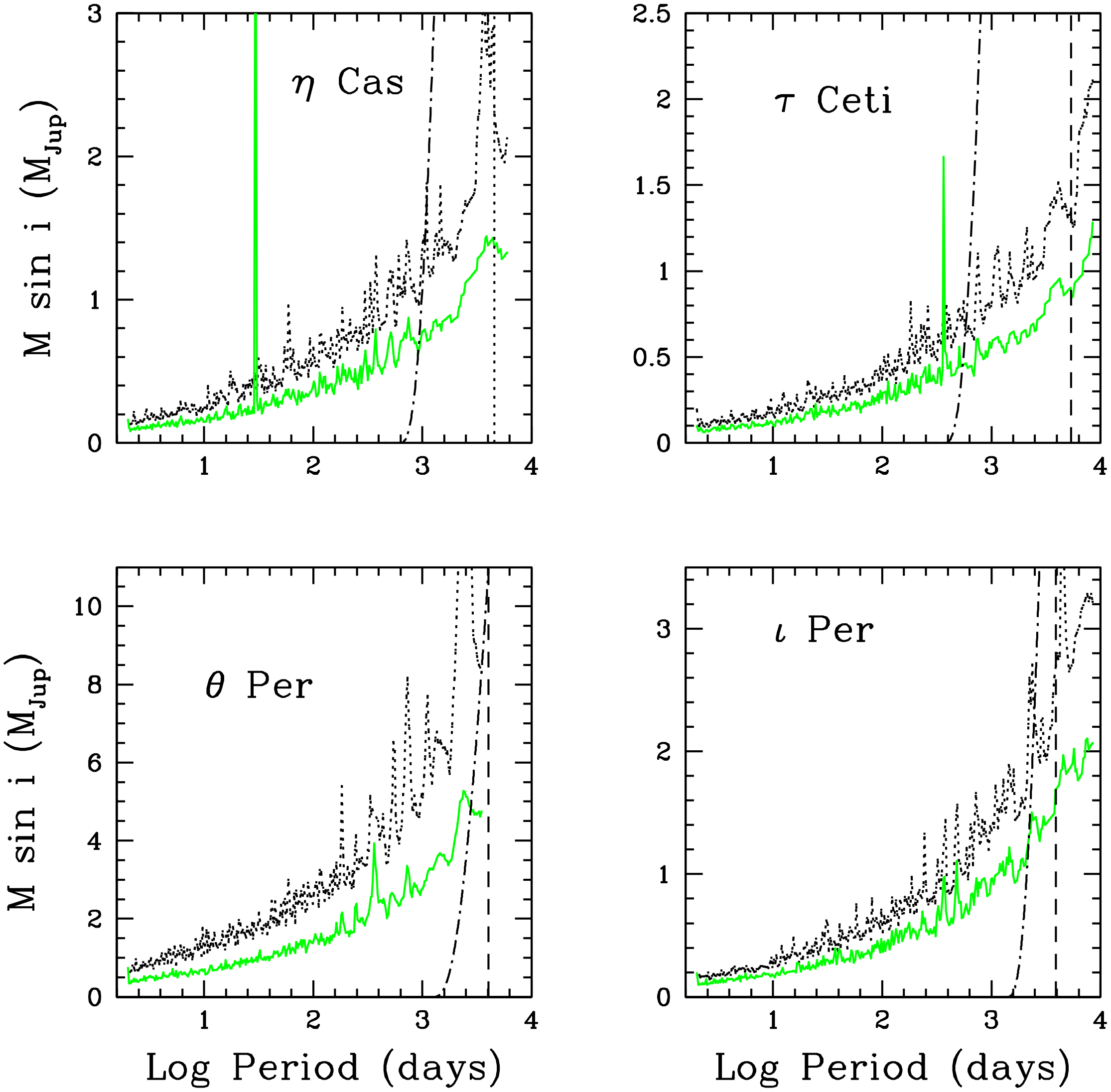

FIG. 4.— Planetary companion limits for η Cas, τ Cet, θ Per, and ι Per. The vertical dashed line indicates the 11.87 yr orbital period of Jupiter. Planets in the parameter space above the plotted points are excluded at the 99% confidence level. The solid line represents the companion limits for the zero-eccentricity case, and the dotted line is for the case of $e = 0.6$. The region left of the dot-dashed line represents the set of perturbers at $e = 0.2$ which would disrupt the habitable zone.

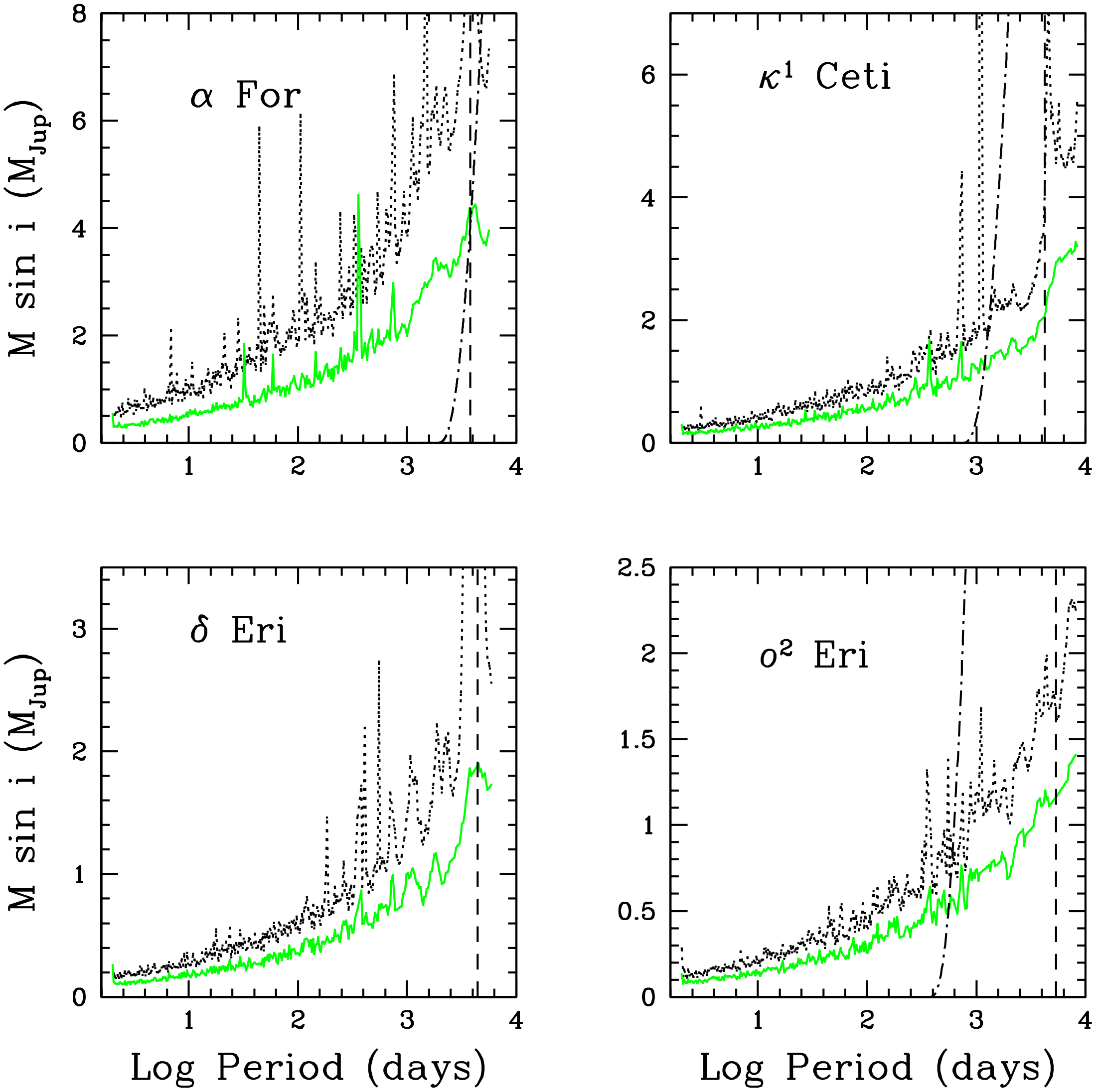

FIG. 5.— Same as Figure 4, for α For, κ^1 Cet, δ Eri, and o^2 Eri.

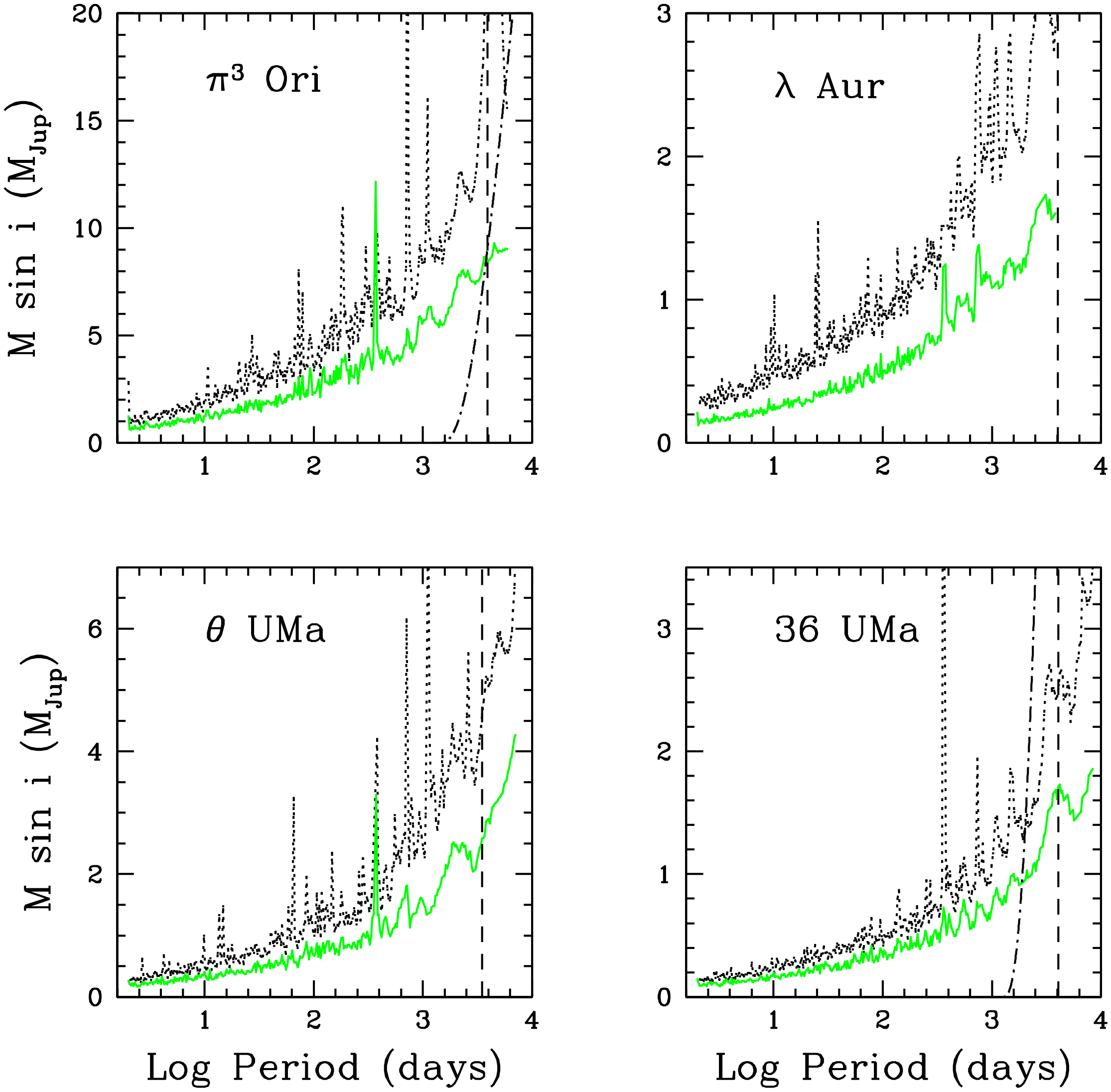

FIG. 6.— Same as Figure 4, for π^3 Ori, λ Aur, θ UMa, and 36 UMa.

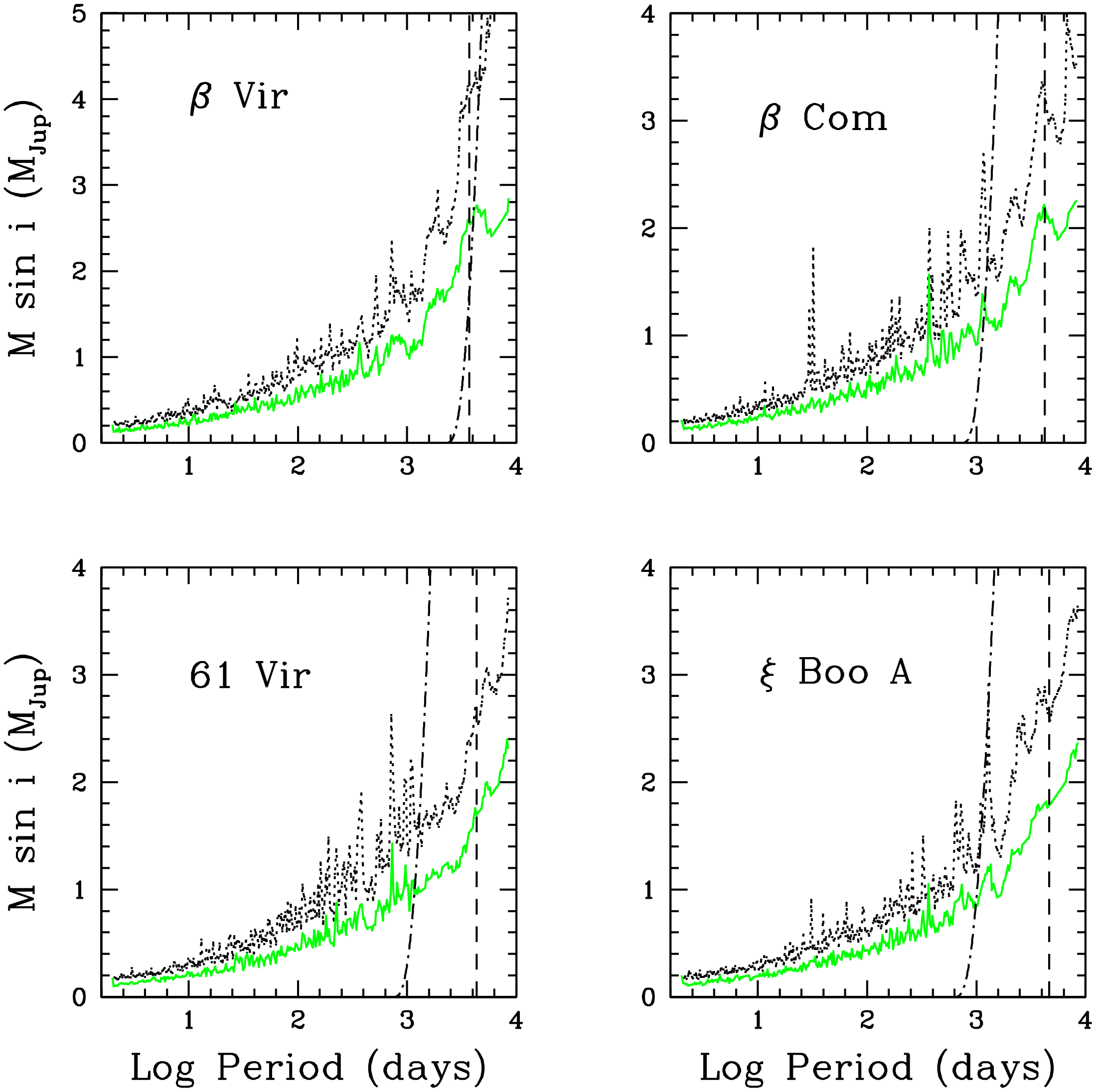

FIG. 7.— Same as Figure 4, for β Vir, β Com, 61 Vir, and ξ Boo A.

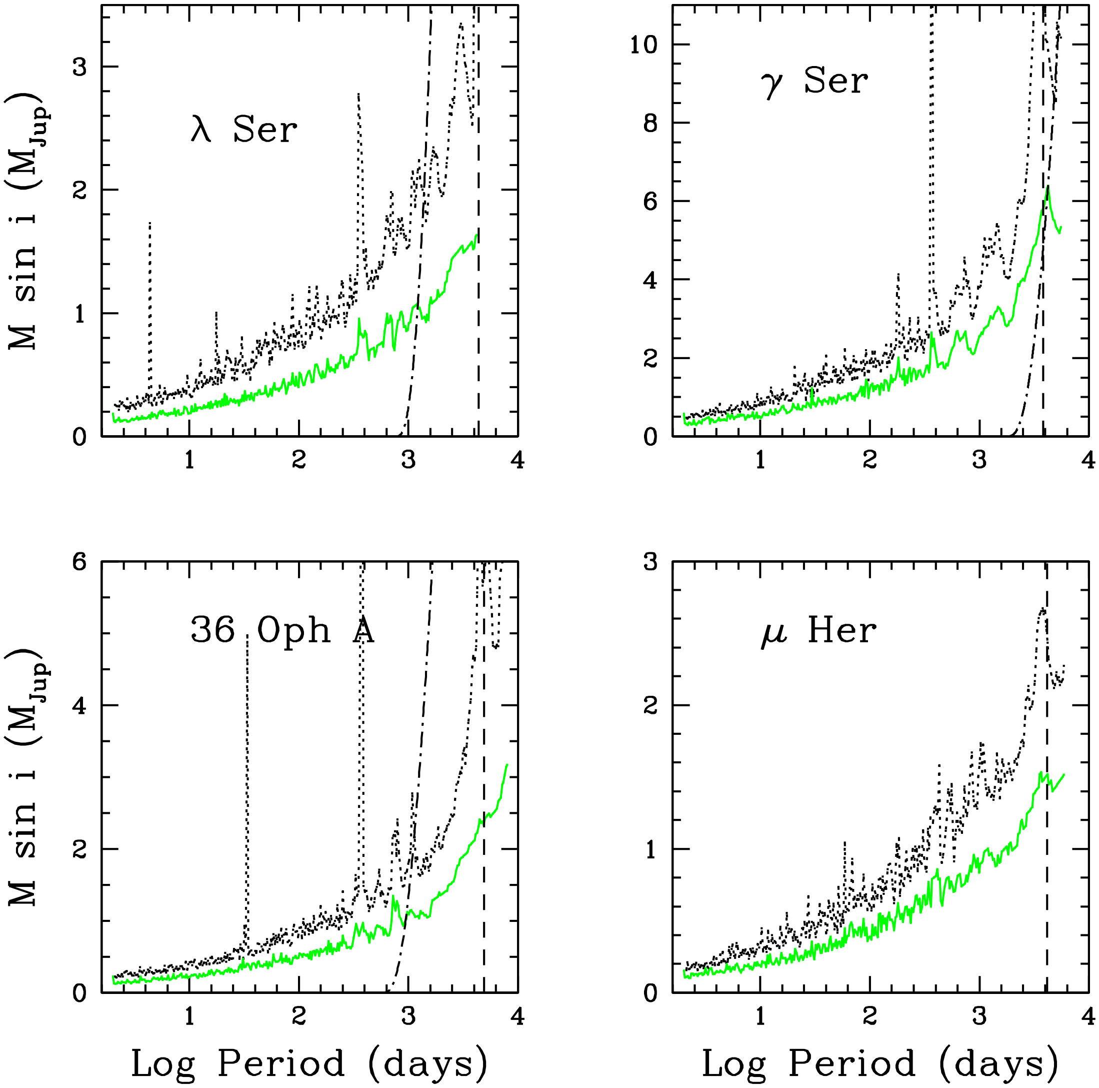

FIG. 8.— Same as Figure 4, for λ Ser, γ Ser, 36 Oph A, and μ Her.

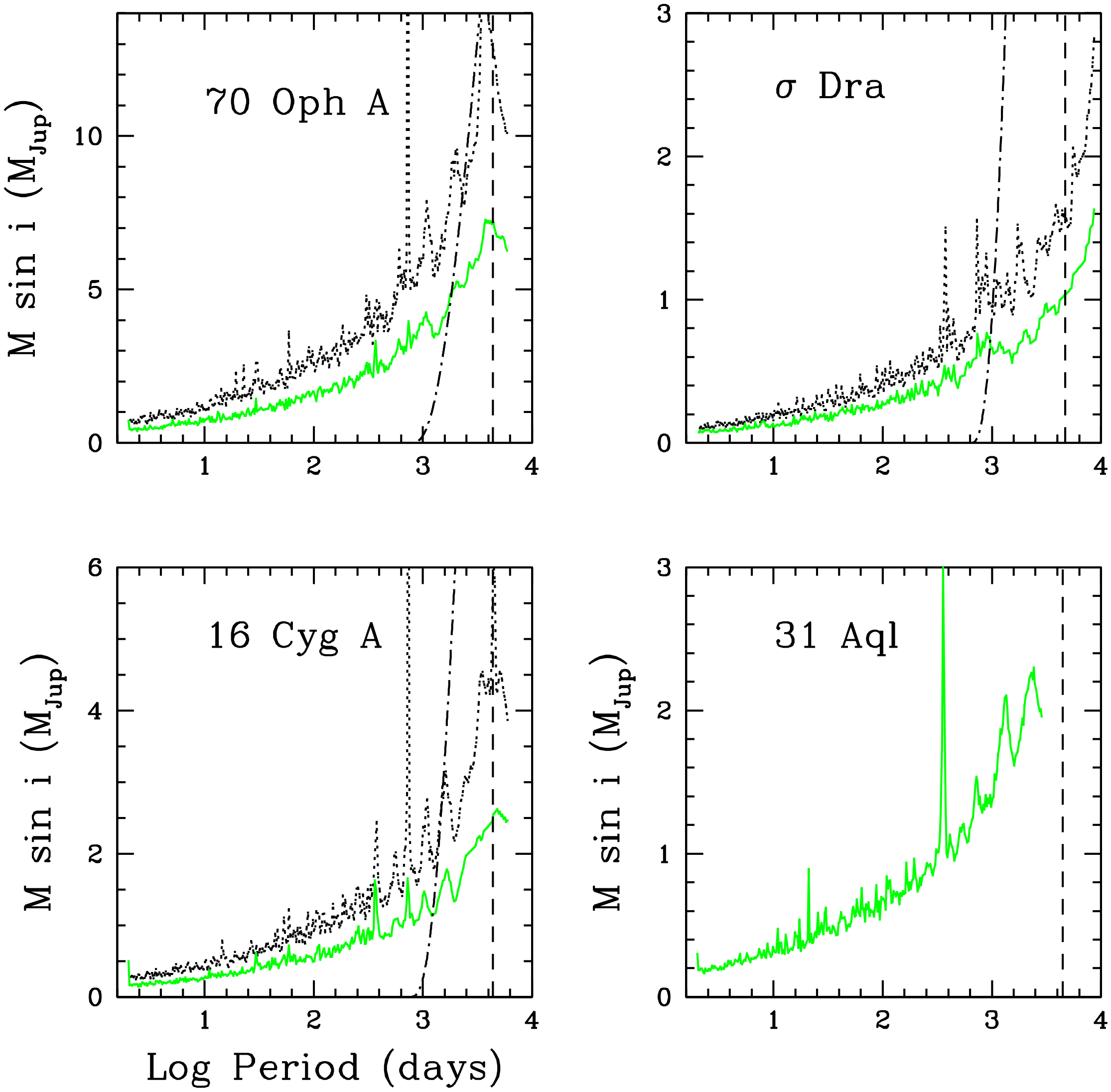

Fig. 9.— Same as Figure 4, for 70 Oph A, σ Dra, 16 Cyg A, and β Aql.

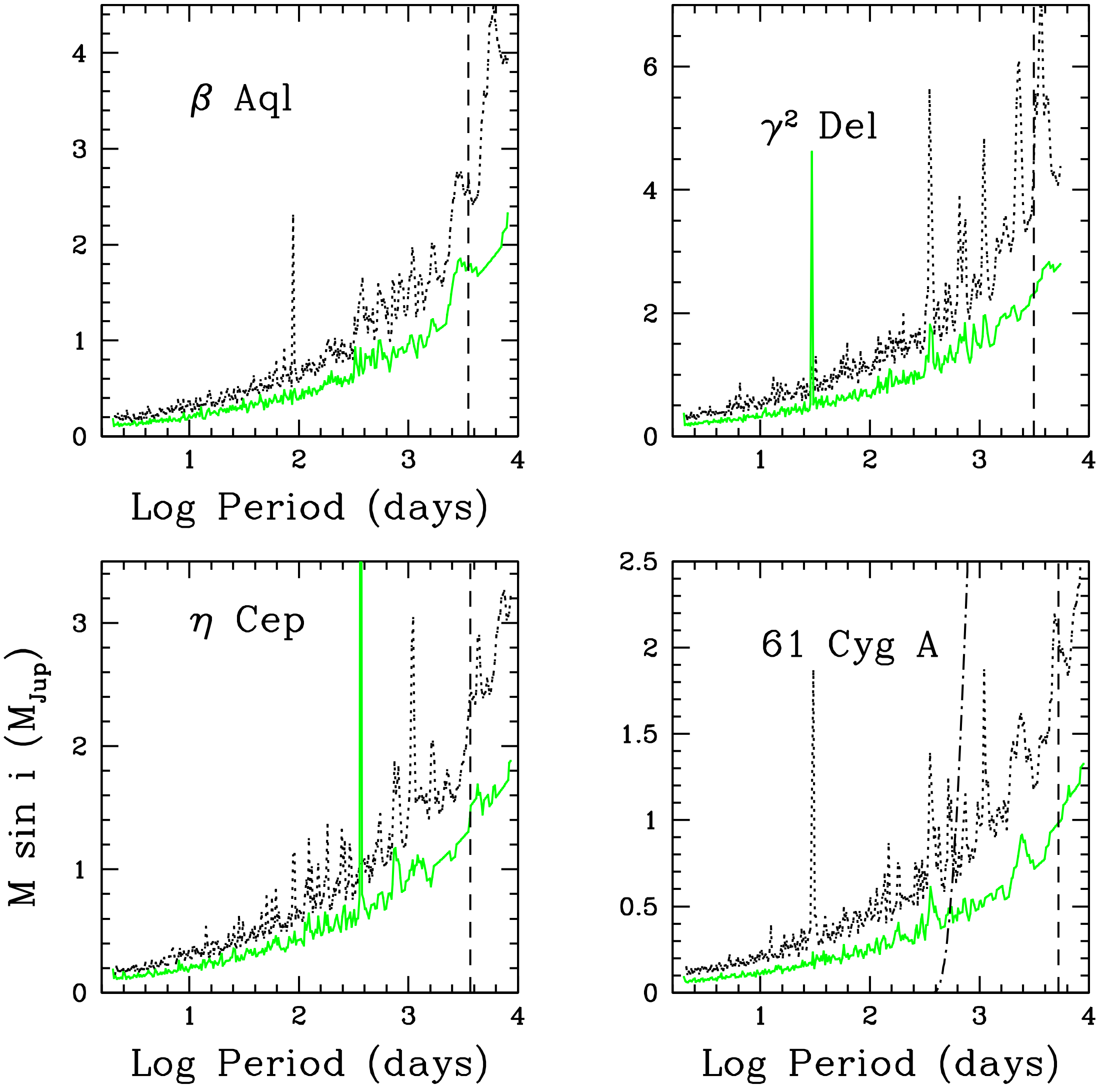

FIG. 10.— Same as Figure 4, for 31 Aql, γ^2 Del, η Cep, and 61 Cyg A.

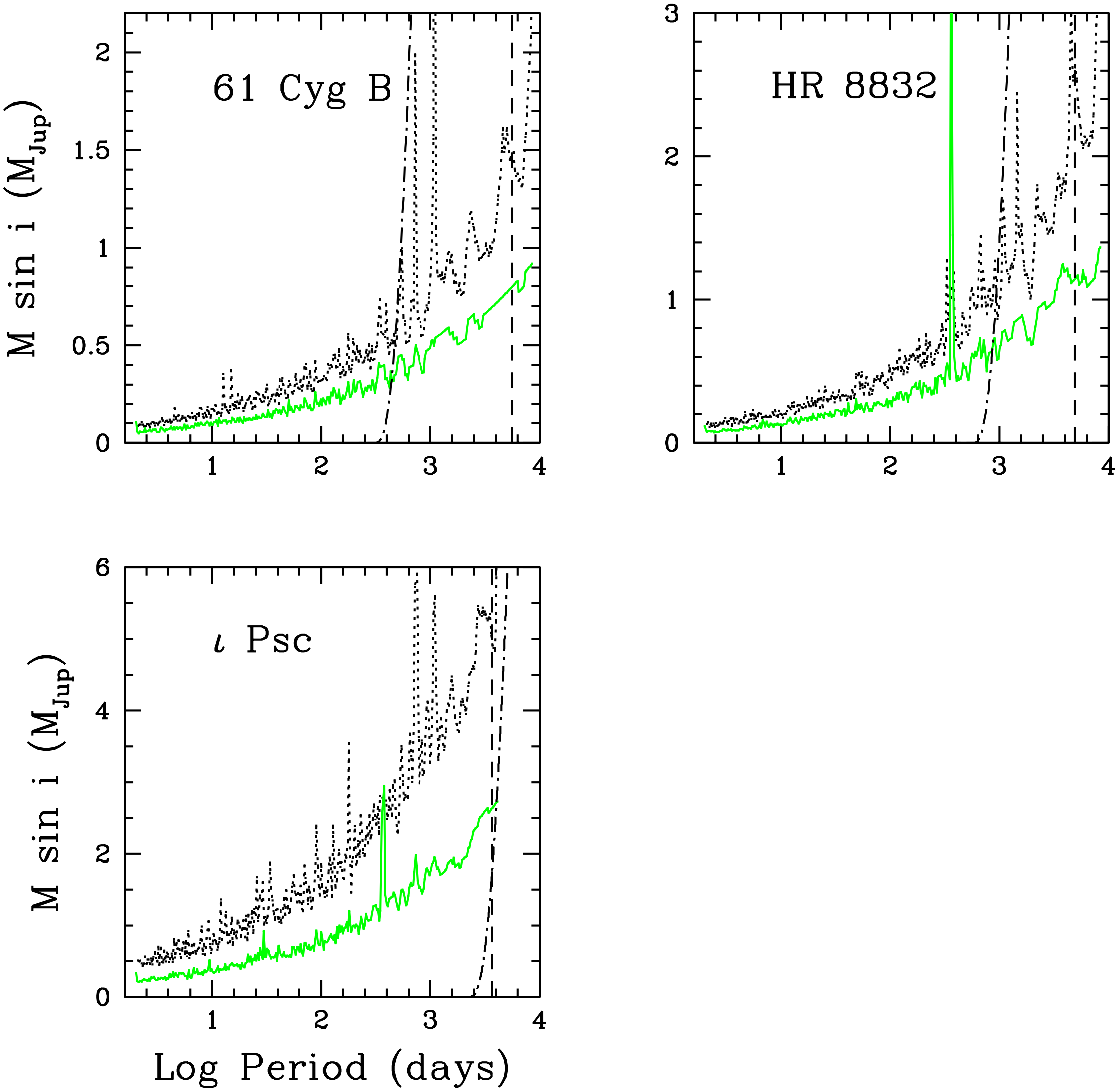

FIG. 11.— Same as Figure 4, for 61 Cyg B, HR 8832, and ι Psc.

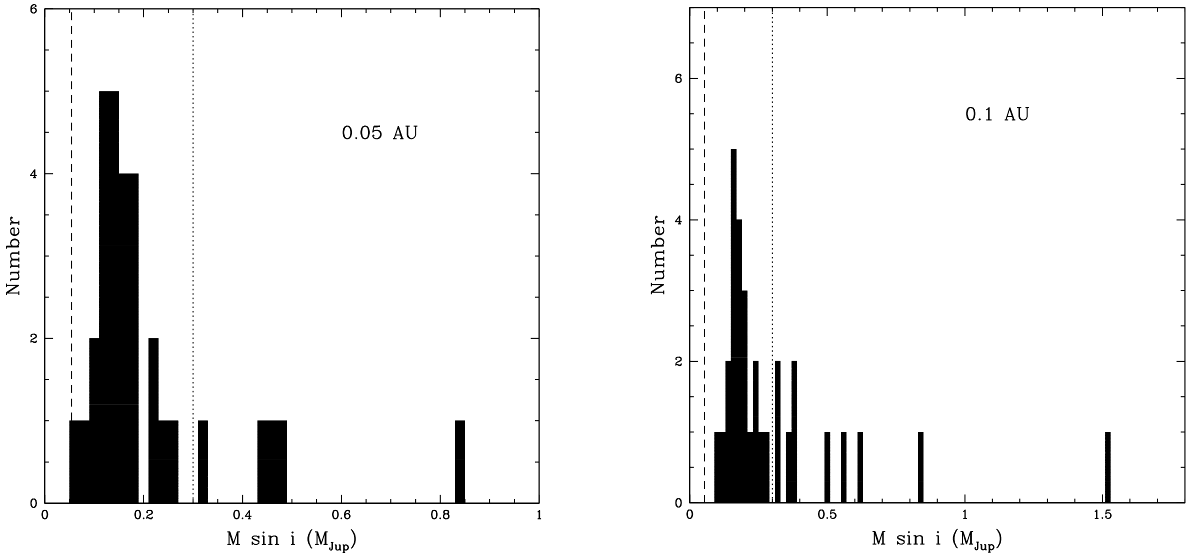

Fig. 12.— Histogram showing the lowest M sin i of planets ruled out at semimajor axes of 0.05 AU (left panel) and 0.1 AU (right panel). The dotted vertical line indicates the mass of Saturn, and the dashed line indicates the mass of Neptune.

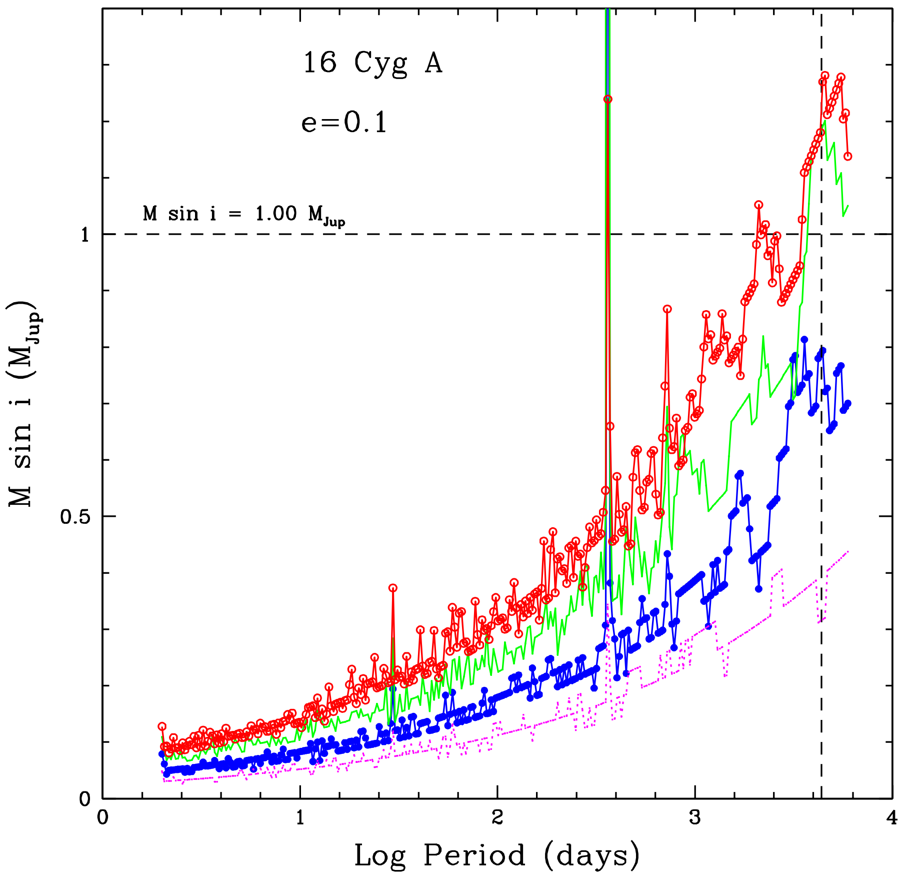

Fig. 13.— Planetary companion limits for 16 Cyg A, using simulated data matching our observation times, but with an rms of 14 m s^{-1} (red, open circles), 11 m s^{-1} (green, solid line), 8 m s^{-1} (blue, filled circles) and 5 m s^{-1} (magenta, dotted line). The vertical dashed line indicates the 11.87 yr orbital period of Jupiter. Planets in the parameter space above the plotted points are excluded at the 99.9% confidence level. This shows that a Jupiter analog could be ruled out at the 99.9% level with a sufficiently long baseline of data similar in quality to the McDonald Observatory phase 3.